Tailoring the Properties of Fe−Fe3C Nanocrystalline Particles Prepared by Sonochemistry

S. I. Nikitenko,[†] Yu. Koltypin,[‡] I. Felner,[§] I. Yeshurun,[‡] A. I. Shames,[||] J. Z. Jiang,[⊥]
V. Markovich,[||] G. Gorodetsky,[||] and A. Gedanken*,[‡]

Institute of Physical Chemistry, RAS, Leninskii Pr.31, 117915 Moscow, Russia, Bar-Ilan University,
Ramat-Gan, 52900, Israel, Racah Institute of Physics, Hebrew University, Jerusalem, Israel, Ben-Gurion
University of the Negev, P.O. Box 653, 84105 Beer-Sheva, Israel, and Department of Physics, Building 307,
Technical University of Denmark, DK-280, Lyngby, Denmark

Received: August 11, 2003; In Final Form: March 31, 2004

Air-stable Fe/Fe3C nanocrystalline particles have been prepared by sonicating Fe(CO)5 in diphenylmethane solutions under argon and subsequently annealing the amorphous as-prepared product in an inert atmosphere. Changing the sonication conditions and annealing temperature allows control of the size of the particles, as well as their composition and magnetic properties. Material obtained under appropriate conditions possesses a high saturation magnetization close to that of bulk iron (M_s/M_0 = 0.97−1.06) and good, soft magnetic properties (H_C = 0.50−0.05 A m^{-1}). Nanocrystalline particles have a core−shell structure where a coating of Fe3C and carbon protects the body-centered cubic Fe in the core from oxidation.

Introduction

Carbon-coated soft magnetic nanoparticles are of great interest in potential applications to perpendicular magnetic recording,[1] highly sensitive magnetic sensors,[2] toners,[3] imaging reagents,[4] and magnetic carriers.[5] The carbon shell protects metal nanoparticles from oxidation and reduces the magnetic coupling between the magnetic bits. Carbon-coated iron nanoparticles are of particular interest since iron has the highest magnetic moment among the 3d transition ferromagnetic metals. Iron nanoparticles coated with carbon have been prepared by different methods, such as arc-discharge,[3] laser-induced pyrolysis,[6] thermal carbonization,[7] ion-beam sputtering,[8] and thermal annealing of the mixture of iron and diamond nanoparticles at 1700 °C.[9] All these processes need high temperatures and yield mixture of products. Saturation magnetization of prepared materials does not exceed 9.95×10^5 A m^{-1}.

Amorphous iron nanoparticles can be prepared by Fe(CO)5 thermolysis at 190 °C[10] or sonolysis at room temperature[11] in hydrocarbon solutions. The chemical effects of ultrasound are related to acoustic cavitation, i.e., formation, pulsation, and, under appropriate conditions, implosive collapse of microbubbles in liquids.[11−13] Iron nanoparticles produced by sonochemistry in hydrocarbons are not stable, since they have no protective shell on the surface.

Recently, air-stable iron nanoparticles coated with cementite Fe3C and carbon have been prepared by sonolysis of Fe(CO)5 in diphenylmethane (DPhM) followed by thermal treatment of the as-prepared material under argon.[12−13] The obtained material exhibits an unusually strong saturation magnetization (M_s) despite the presence of about 20 mol % of Fe3C. It was found that the magnetic properties of the obtained material are strongly dependent on the annealing temperature of the solid sonication product. Thus, Fe/Fe3C nanocrystalline particles can be tailored to meet the requirements of various specific applications.

The objective of this work has been to investigate the effect of sonolysis and thermal treatment conditions on chemical composition, magnetic properties, and particle size of Fe/Fe3C nanocrystalline material.

Experimental Section

Diphenylmethane (>99%, Fluka) and Fe(CO)5 (99.5% STREM) were used without additional purification. A Fe(CO)5 solution of the desired concentration in DPhM was sonicated in the presence of argon by means of a Sonics and Materials ultrasonic device with a direct immersion titanium horn (working frequency, 20 kHz; electric power of generator, 600 W; irradiation surface area of the horn, 1 cm^2). The volume of the sonicated solution was 100 mL. The absorbed acoustic power, measured by the thermal probe method,[14] was found to be equal to 0.45 W/mL. The temperature was maintained during sonication by a Julabo FT901 cooler. As a rule, sonolysis was performed for 1 h at 25−28 °C. All sonochemical experiments were carried out under argon.

The black solid product of sonication was removed by centrifugation, washed three times with pentane inside a N2-filled glovebox, and dried under vacuum at room temperature. Annealing of the solids was performed in an argon flow (99.996%) for 2 h.

XRD was recorded on a Bruker AXS D* Advanced powder X-ray diffractometer (Cu Kα radiation, λ = 0.154 18 nm). An XRD spectrum of the as-prepared material was measured in a tightly closed cell to avoid sample contact with air. Measurements of annealed samples were performed without special precautions.

Low-resolution TEM were obtained with a JEOL-JEM100SX electron microscope with 80−100 kV accelerating voltage. High-resolution TEM images were obtained by employing a JEOL-3010 device with 300 kV accelerating voltage.

Mössbauer spectroscopy (MS) studies were carried out using a conventional constant acceleration spectrometer (50 mCi

* Corresponding author. Fax: +972-3-5351250. E-mail: gedanken@ mail.biu.ac.il.
† RAS.
‡ Bar-Ilan University.
§ Hebrew University.
|| Ben-Gurion University of the Negev.
⊥ Technical University of Denmark.

Fe−Fe$_3$C Nanocrystalline Particles

J. Phys. Chem. B, Vol. 108, No. 23, 2004 **7621**

TABLE 1: Elemental Analysis of Iron Samples before and after Annealing for 2 h in Pure Argon[a]

temp of annealing (°C)	C (atom %)	H (atom %)	temp of annealing (°C)	C (atom %)	H (atom %)
as-prepared	35.6	33.3	800	7.1	0
300	29.3	7.8	850[b]	2.1	0
400	22.1	3.1	700[c]	54.3	3.0
700	16.5	0			

[a] Time of sonolysis, 1 h. Temperature of sonolysis, 25−28 °C. [b] Time of annealing was 5 h. [c] As-prepared sample was obtained by sonication at 90 °C.

[57]Co:Rh source). MS spectra were least-squares-fitted with one or more subspectra. All MS measurements were performed at 300 K.

Magnetic measurements were performed on a sample of Fe−FeC that was introduced into a plastic capsule. Measurements at room temperature and low temperature were performed using a Quantum Design MPMS SQUID magnetometer (Quantum Design MPMS-5S).

Magnetization was measured at fixed temperatures (5, 10, 20, 300 K) as a function of the external field being swept up and down ($-20\,000$ Oe $< H_{applied} < 20\,000$ Oe, in steps of 200 Oe).

The margin of error in weighing the samples for magnetic measurements is estimated at least by 10%. This is because we could not weigh more than 2 mg. Heavier weights caused the measurements to go off scale. The balance could measure with an accuracy of 0.1 mg. This introduces already a 10% error. The error might be even higher. The saturation magnetization of commercial iron powder ($d \leq 5\ \mu m$) measured by the same procedure was found to be equal to 1.6×10^6 A m^{-1}, which is very close to the M_0 value for bulk Fe (1.7×10^6 A m^{-1}).

The electrical resistivity dependence on temperature was measured using a customary four-point method in the temperature range of 20−300 K. The dried powders of the samples were pressed into cylindrically shaped samples of 2.4 mm in diameter and 5 mm in length with a pressure 600−700 Mpa. The separation between the voltage contacts was about 2.5 mm. Electrodes were formed with heat treatment type silver paint.

Room-temperature ferromagnetic resonance (FMR) spectra were recorded using a standard electron paramagnetic resonance spectrometer working at 9.25 GHz.

The thermogravimetric analysis (TGA) and differential scanning calorimetric analysis (DSC) were performed by using a Mettler Toledo TGA/SDTA 851 and DSC-25/TC-15 devices, respectively, under pure nitrogen flow.

X-ray photoelectron spectroscopy (XPS) were recorded using a AXIS, HIS 165, ULTRA (Kratos Analytical) device. The XPS data were acquired for Fe 3p, C 1s, and O 1s photoelectron emission. Surface etching of the samples was performed by argon plasma.

Elemental analysis was carried out by an Eager 2000 CHN analyzer. FTIR spectra were recorded in KBr pellets using an Impact 410 Nicolet spectrometer.
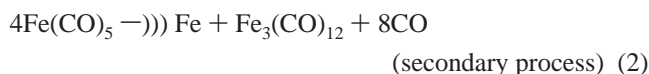
Results and Discussion

Elemental, FTIR, and TGA/DSC Analysis. The initial orange color of the solution changes to black under ultrasonic treatment. About 250 mg of the black solid is removed from 100 mL of a 1 M Fe(CO)$_5$ solution after 1 h of sonolysis. The as-synthesized material is pyrophoric upon its exposure to air. The results of elemental analysis are presented in Table 1 for as-prepared and annealed samples. Annealing causes a dramatic

drop in the C and H content, but some amount of carbon is still present even after 5 h of heating at 850 °C. Annealed powders are stable in contact with air.

Obviously, carbon and hydrogen in as-prepared material come from the sonication product of DPhM. Recently, it was found[15] that sonolysis of neat DPhM yields a sonopolymer with a structure similar to that of cross-linked polystyrene. The FTIR spectrum of the as-prepared material exhibits absorption bands at 3060−3020, 2900−2850, and 1100−1000 cm^{-1} assigned to C−H stretch vibrations in aromatic and aliphatic groups and *p*-substituted phenyls, respectively.[16] Thus, the FTIR spectrum confirms the presence of some kind of polymerized aromatics in the as-prepared product of sonolysis.

From the Table 1, it is seen that C and H concentrations are considerably increased in the solid sample when the temperature of sonication is increased to 90 °C. This phenomenon can be related to the mechanism of DPhM sonolysis. It was assumed that the sonopolymer is formed due to the dissociation of DPhM molecules inside the cavitating bubble, followed by the recombination and scavenging of the sonochemically formed radicals.[15] An increase in the temperature of sonolysis causes an increase of DPhM vapor pressure inside the bubble. Thus, the yield of the sonopolymer also increases with the temperature of the solution.

The sonicated solution is green after removal of the solids. The IR spectrum of the sonicated solution shows the absorption bands at 2010−2050 and 1830−1870 cm^{-1} characteristic for C−O stretch vibrations of terminal and bridging carbonyl groups, respectively, in a complex Fe$_3$(CO)$_{12}$.[16] Formation of Fe$_3$(CO)$_{12}$ also has been observed during Fe(CO)$_5$ sonolysis in alkane solutions.[17] One can conclude that the mechanism of Fe(CO)$_5$ sonolysis in DPhM solutions can be presented by the following scheme:

$$Fe(CO)_5 \longrightarrow))) Fe + 5CO \quad \text{(major process)} \quad (1)$$

$$4Fe(CO)_5 \longrightarrow))) Fe + Fe_3(CO)_{12} + 8CO$$
$$\text{(secondary process)} \quad (2)$$

where the symbol "$\longrightarrow$)))" corresponds to the reactions under the effect of acoustic cavitation. An increase in the temperature of sonication to 90 °C causes the disappearance of Fe$_3$(CO)$_{12}$, probably due to its thermal decomposition.

Figures 1 and 2 display TGA and DSC curves, respectively, for the as-prepared sample obtained by sonolysis at 30 °C. The TGA curve exhibits a two-stage mass loss at 150−230 and 320−350 °C of about 12.5 and 5.3 wt %, respectively. The total mass loss found from the TGA curve is in good agreement with elemental analysis data (14.7 wt % estimated mass loss). Taking into account that the as-prepared material contains about 21 wt % of the sonopolymer (Table 1), it can be assumed that some part of the sonolysis product of DPhM is decomposed to elemental carbon or reacted with an amorphous iron during the annealing procedure. The DSC curve is characterized by several broad endothermic peaks in the 150−360 °C range and a sharp exothermal effect around 480 °C. The endothermic effects and the corresponding mass loss processes are expected to be related to following processes: (i) organic sonopolymer thermolysis and (ii) inreaction of the amorphous iron with the sonopolymer. The sharp exothermal peak most likely corresponds to iron crystallization. The crystallization temperature ($\sim$480 °C) for amorphous iron obtained from DPhM solutions is much higher than that for amorphous iron obtained from alkane solutions ($\sim$320 °C).[17,18] It can be assumed that the product formed as a result
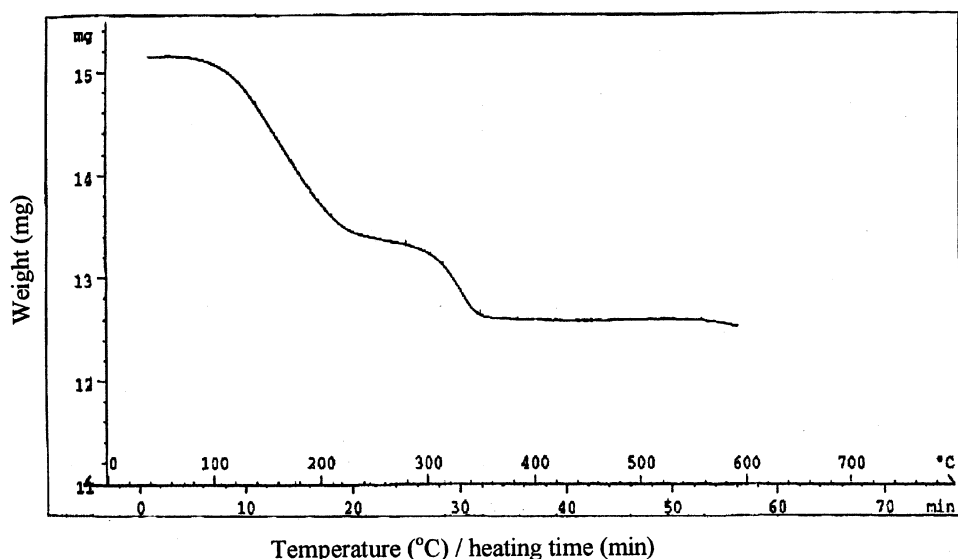
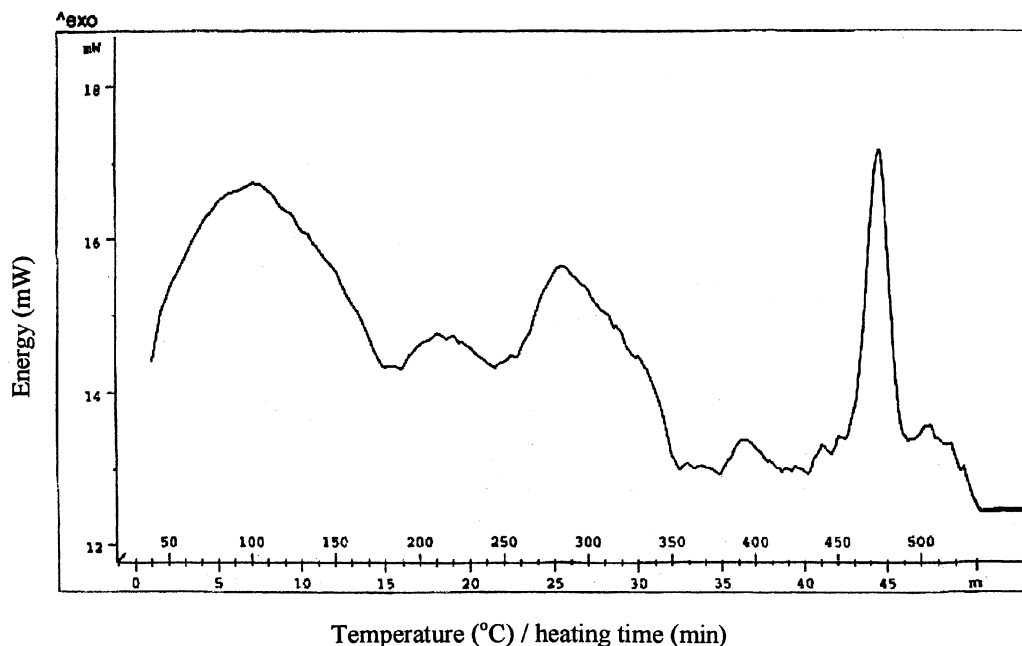**Figure 1.** TGA curve for as-prepared sample.

Figure 2. DSC curve for as-prepared sample.

of the annealing process is crystallized at the higher temperature than that of amorphous iron.

XRD Study. The as-prepared product is X-ray amorphous, as follows from XRD data shown in Figure 3a. A sample annealed at 300 °C consists of the magnetite Fe_3O_4 and cementite Fe_3C, according to the XRD spectrum presented in Figure 3b. The material obtained by annealing at 400 °C exhibits the XRD patterns characteristic of body-centered cubic (bcc)-Fe, Fe_3C, and some admixtures of maghemite Fe_2O_3 (Figure 3c). XRD data of the sample obtained at 700 °C reveal only the presence of bcc-Fe and Fe_3C (Figure 3d). The XRD spectrum of the sample heated at 800 °C is similar to that obtained at 700 °C and is not shown in Figure 3.

XRD measurements clearly indicate that particle stability and their chemical composition depend considerably on the annealing temperature. Particles obtained at 300 °C are unstable with respect to oxidation. Iron is totally oxidized to Fe_3O_4 in contact with air. At the same time, Fe_3C formed at 300 °C shows a strong resistance to oxidation. Iron particles annealed at 400

°C and higher are already air stable. Only small admixtures of Fe_2O_3 can be detected by the XRD method in the sample annealed at 400 °C. The material obtained under sonication at 90 °C consists of Fe_3C and admixtures of bcc-Fe according to the XRD spectrum shown in Figure 3e.

Mössbauer Spectroscopy Analysis. The MS spectrum of as-prepared material exhibits a doublet typical of the superparamagnetic nanoparticles. The MS spectrum of the material prepared at 300 °C exhibits peaks characteristic of Fe_3O_4 and Fe_3C. The MS spectra presented in Figure 4 reveal that the samples annealed at 400 and 700 °C contain bcc-Fe, iron carbide Fe_3C ($H_{eff} = 208 \pm 5$ kOe), and small amounts of Fe_2O_3. Particles prepared by annealing at 800 °C have no iron oxide admixtures. Long-time annealing at 850 °C causes the disappearance of Fe_3C. The MS of the high-temperature sonication product (90 °C), after annealing at 700 °C, is characterized by a high content of carbon consisting of Fe_3C. Only small amounts of bcc-Fe are detected in the MS for this product. The chemical composition of the particles calculated from MS data is

Fe−Fe₃C Nanocrystalline Particles

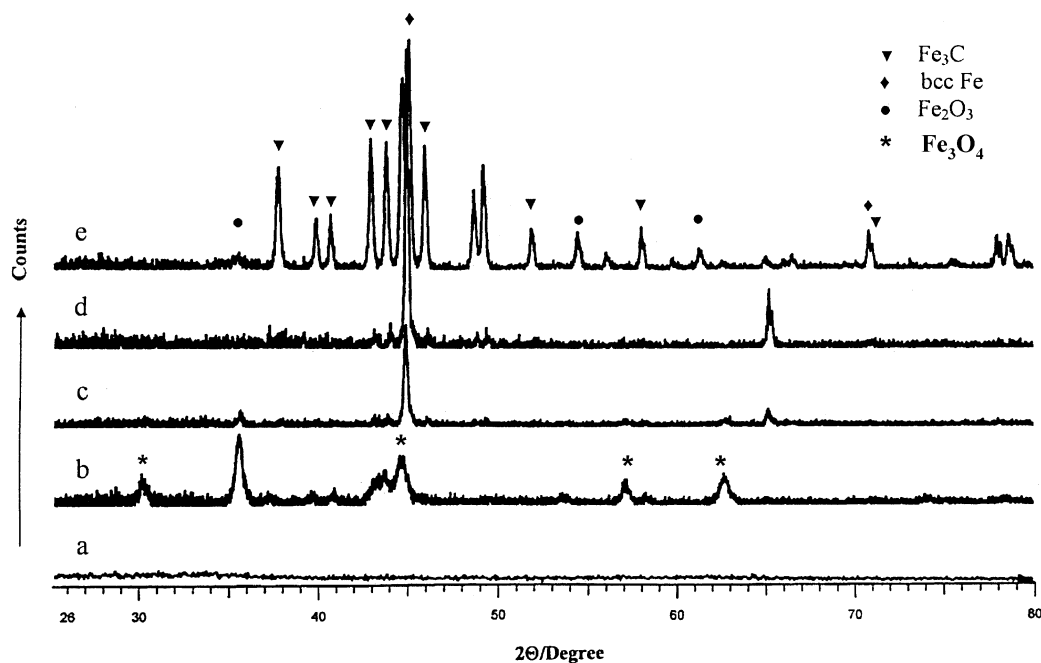*J. Phys. Chem. B, Vol. 108, No. 23, 2004* **7623**

Figure 3. XRD data for (a) as-prepared material and materials annealed at (b) 300 °C, (c) 400 °C, (d) 700 °C, and (e) 700 °C (sample obtained by sonication at 90 °C): (▼) bcc-Fe, (◆) Fe₃C, (*) Fe₃O₄, and (†) Fe₂O₃.
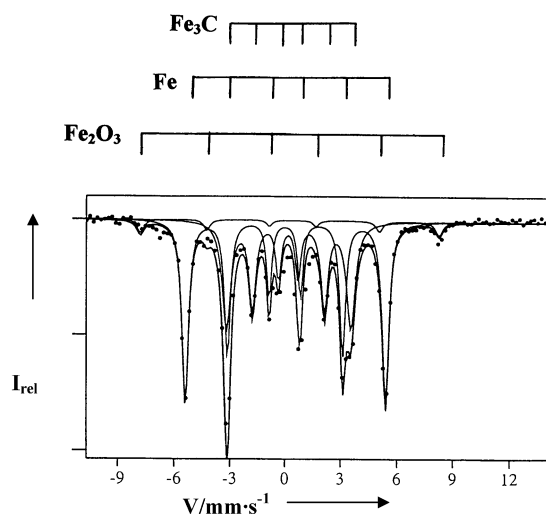

Figure 4. Moessbauer spectra of material annealed at 700 °C.

TABLE 2: Chemical Composition of the Nanocrystalline Particles Obtained from MS Data

temp of annealing (°C)	Fe (atom %)	Fe$_C$[a] (atom %)	Fe₃O₄ (atom %)	Fe₂O₃ (atom %)	C$_{el}$[b] (atom %)
300	0	62	38	0	8.6
400	36	57	0	6.5	3.1
700	53	42	0	5.0	2.5
850[c]	100	0	0	0	2.1
700[d]	10	90	0	0	24.3

[a] Fe$_C$, concentration of iron in the form of iron carbide Fe₃C. [b] [C$_{el}$] = ∑[C] − ¹/₃[Fe$_C$], where ∑[C] is total carbon concentration form the Table 1. [c] Time of annealing was 5 h. [d] As-prepared sample was obtained by sonication at 90 °C.

presented in Table 2. The results of the MS study are in a good agreement with XRD data.

XPS Study. The results of XPS measurements for the samples prepared at 400 and 700 °C are presented in Table 3. The surface concentration of carbon obtained by XPS is much higher than the average carbon concentration obtained by elemental analysis.

TABLE 3: XPS Measurements of Fe, C, and O Surface Concentrations for Annealed Samples Using Fe 3p (55.350 eV), C 1s (284.350 eV), and O 1s (530.125 eV) Signals, Respectively

etching time (min)	surface concn (atom %)		
	Fe	C	O
Annealed at 400 °C			
0	14.0	66.0	20.0
12	33.5	49.2	17.3
24	35.8	48.6	15.6
Annealed at 700 °C			
0	13.6	75.6	10.8

It can be assumed that carbon or iron carbide form the shell on the iron particle's surface. Etching for ∼12 min in an argon plasma causes a decrease of carbon concentration and an increase of iron concentration on the particle's surface. Further etching does not change the results significantly. Etching for 12 min under the same conditions corresponds to ∼5 nm of sputtered shell width at the applied conditions of sputtering. It is worth noting that etching in the presence of argon prevents the iron surface from being oxidized by atmospheric oxygen. Thus, XPS data allow the estimation of the shell thickness equal to approximately 5 nm composed from Fe₃C and C, which protect the iron from oxidation.

Electrical Resistivity. The dependence of electrical resistivity, ρ, versus temperature, is shown in Figure 5 for the samples annealed at 400 and 700 °C. The resistivity curve of the material heated at 800 °C is similar to that obtained at 700 °C and is not shown in Figure 5. The sample obtained at 400 °C exhibits a metal-like contribution ($d\rho/dT > 0$) at low temperatures of 50−120 K. The value of ρ is increased with time for this sample at temperatures lower than 200 K. Presumably, the above effects are related to a relatively poor isolation of the iron particles by the thin, protecting shell. The nature of the rather small increase in the resistivity ($d\rho/dT < 0$) at $T < 50$ K is unclear at this moment. The tunneling mechanism through the isolating layer can also be held responsible for the increase in the low-temperature resistivity.[19] In the case of manganites, at low
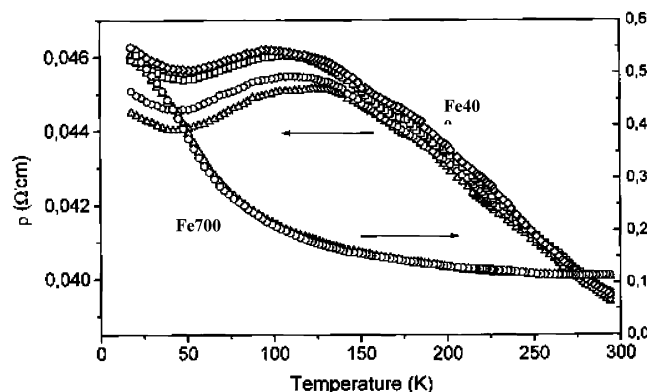
Figure 5. The temperature dependence of electrical resistivity, ρ, with time. The time intervals after preparing pressed samples for resistivity measurements are pointed.
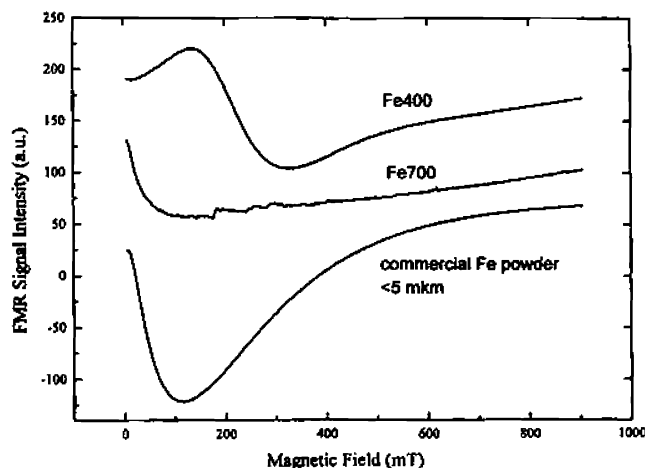

Figure 6. FMR spectra polycrystalline samples: (upper) nanocrystalline sample annealed at 400 °C, $n = 9.263$ GHz; (middle) nanocrystalline sample annealed at 700 °C, $n = 9.258$ GHz; (lower) commercial metallic iron powder, $n = 9.399$ GHz

temperatures ($T < 50$ K) an increase in resistivity is found, which has been attributed to the Coulomb blockade in small particles.[20] An increase in the annealing temperature to 700−800 °C improves the particles encapsulation, resulting in a semiconducting-like behavior of the shell (decrease of ρ with temperature) and higher values of ρ compared with the results obtained for the sample annealed at 400 °C. This remarkable increase in the resistivity of about 10 times that of the low temperature (400 °C) annealed product is caused by enhancement in the potential barrier between particles due to the protective shell. The time stability of the resistivity is also improved for the 700−800 °C annealed product. Thus, the measurements of the electrical resistivity confirm the existence of a protecting layer on the surface of the particles.

The electrical resistance of the sample depends on the resistance of Fe/Fe$_3$C nanocrystalline materials, the resistance of carbon coating (depending on the thickness of this coating), the interface between Fe/Fe$_3$C nanocrystalline materials and C-coating, and the electrical contact between different coated nanoparticles. Obviously, annealing at different temperatures may change the relative contribution to the electrical resistance of the above contributions. Moreover, phase transformation may be produced by annealing at $T > 600$ K. Such a transformation was found to occur in fine nanoparticles of Fe/Fe$_3$C under a flow of argon.[21] Moreover, the Fe$_3$C fine nanoparticles oxidize to γ-Fe$_2$O$_3$ and carbon dioxide at 610 K.[21] High-resolution transmission electron microscope images[22] have shown that the annealing at 600 K changes both the thickness of the coating and the interface between the particle and the coating. Namely, TEM images have shown that as-made iron particles are coated by a thick layer of amorphous carbon and that the interface between the amorphous layer and the metal particle is distinct.[22] Such images after annealing have shown that particles are covered by more than four graphitic layers, rather than by an amorphous graphite, and a discrete interface between graphitic coating and the metal particles defines the thickness of the carbon coating.[22] It is obvious that such a transformation may be accompanied by changes in both the magnitude and character of the temperature dependence of the resistivity. The question arising here is the electrical resistivity of the carbon coating itself and the effect of annealing on its resistance. It is well-known that carbon may exist in various allotrophic modifications, differing in the conductivity at room temperature by more than 22 orders of magnitude (from 10^{-18} Ω^{-1} cm^{-1} for diamond to 2.5×10^4 Ω^{-1} cm^{-1} for graphite).[23] The electrical conductivity of amorphous carbon depends strongly on heat treatment.[23] For example, electrical resistivity at room temperature of amorphous carbon films with a different deposition temperature

(from 75 °C up to 350 °C) differs by about 10 orders of magnitude.[23,24] Generally, the temperature dependence of the resistivity in amorphous semiconductors varies as $\rho(T) = A \exp(W/k_BT)$, where A is a constant and W is an activation energy. It should be noted that although the resistivity of all amorphous carbon films exhibit semiconducting behavior ($d\rho/dT > 0$), they did not obey any law particularly well. The above discussion shows that the resistivity of iron particles coated by carbon may be strongly influenced by annealing.

FMR Study. Figure 6 depicts the room-temperature FMR spectra of samples annealed at 400 and 700 °C, compared with the FMR spectrum of commercial iron powder ($d \leq 5$ μm). The FMR spectrum of the 400 °C annealed sample clearly demonstrates the appearance of a ferromagnetically ordered phase. The FMR line is shifted to low fields from the $g \sim 2$ position, due to internal anisotropy fields. The FMR spectrum of the 700 °C annealed sample demonstrates a very broad line centered at zero field. This is a characteristic feature of powdered magnetic metals and resembles the FMR spectrum of commercial micron-sized Fe powder (see Figure 6). One can conclude that magnetic anisotropy parameters for the 700 °C annealed sample exceed those for the 400 °C annealed sample. Such an increase in the magnetic anisotropy may occur due to the increase of the particle size upon annealing. The noise-like feature in the FMR spectrum of the 700 °C annealed sample indicates that the particles are less agglomerated than those heated at 400 °C or commercial iron samples. Well-developed surface coating reduces the agglomeration of magnetic nanoparticles, enabling individual small particles to oscillate in the presence of the 100 kHz modulation field. As mentioned above, the resistivity measurements also indicated the increase in the coating quality on increasing annealing temperature.

TEM Study. Low-resolution TEM images are presented in Figure 7. The as-prepared product consists of nanosized globular agglomerates with very small ($\sim$5 nm) dense particles dispersed inside the globules (Figure 7a). It can be assumed that iron nanoparticles formed from Fe(CO)$_5$ are included in a sonopolymer matrix. The shape and the size of heated particles depend on annealing temperature. Particles heated at 300 and 400 °C have a round shape morphology. Figure 7b indicates that the material annealed at 700 °C is composed mainly of tetragonal and round particles. An increase in the annealing temperature to 800 °C causes the formation of hexagonal and tetragonal particles. Long-time annealing at 850 °C leads to the formation
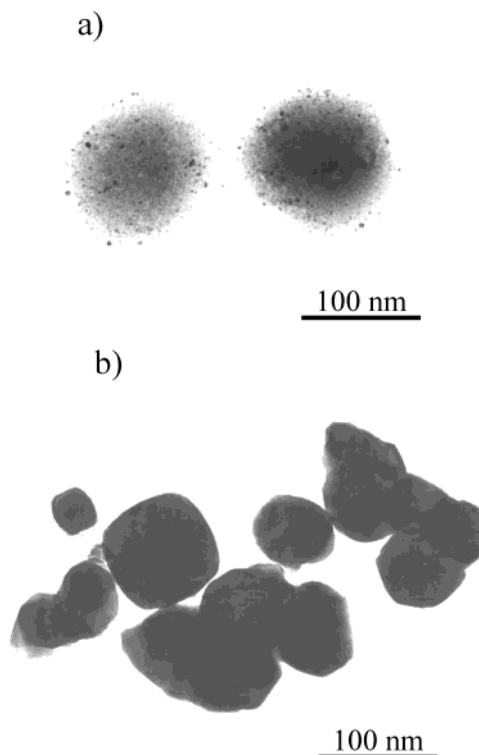
Fe−Fe₃C Nanocrystalline Particles

J. Phys. Chem. B, Vol. 108, No. 23, 2004 **7625**

Figure 7. Low-resolution TEM pictures of (a) as-prepared particles and (b) particles annealed at 700 °C.

TABLE 4: Effect of Annealing Temperature on Particle Size from TEM Measurements

annealing temp, °C	300	400	700	800	850[a]
particle size, nm	10−40	20−100	50−100	70−150	200−300

[a] Annealing time was 5 h.

of relatively big particles with low-symmetry. Particles with a high content of Fe₃C also have rounded symmetry. The particle size estimated from the TEM data increases with the increase in the annealing temperature, as shown in Table 4. The high-resolution TEM picture (Figure 8) confirms that iron nanoparticles are coated by a crystalline shell with a thickness of about 5 nm. The surface coating is composed of a nonlayered crystalline compound, probably Fe₃C, and a layered material with the interlayer distance (Figure 8b) of 0.34 nm typical for graphite.

Magnetic Measurements. The magnetization curve presented in Figure 9 shows that the as-prepared material exhibits superparamagnetic behavior, when no coercivity or saturation magnetization is observed. The annealed materials exhibit a ferromagnetic behavior (Figure presented as supplementary information). Saturation magnetization, M_S; remanentmagnetization, M_R; and coercivity, H_C, are summarized in Table 5 as a function of annealing temperature. It is clearly seen that as the annealing temperature increases, M_S also increases, but M_R and H_C decrease. The change in the magnetic parameters due to the annealing is very dramatic. The coercive force drops by 2 orders of magnitude from 450 Oe for $T = 300$ °C to 4 Oe for $T = 800$ °C. The M_S value increases by almost 250% from $4.4 \times 10^5 \pm 0.5 \times 10^5$ A m⁻¹ at $T = 300$ °C to $1.8 \times 10^6 \pm 0.2 \times 10^6$ A m⁻¹ at $T = 800$ °C as a result of the annealing procedure. We attribute the dependence of magnetic parameters on the annealing temperature to the change in the particle composition, as well as to the particles' size and their morphology. Comparing Tables 2 and 5 shows that the coercive force decreases and saturation magnetization is raised when the iron carbide
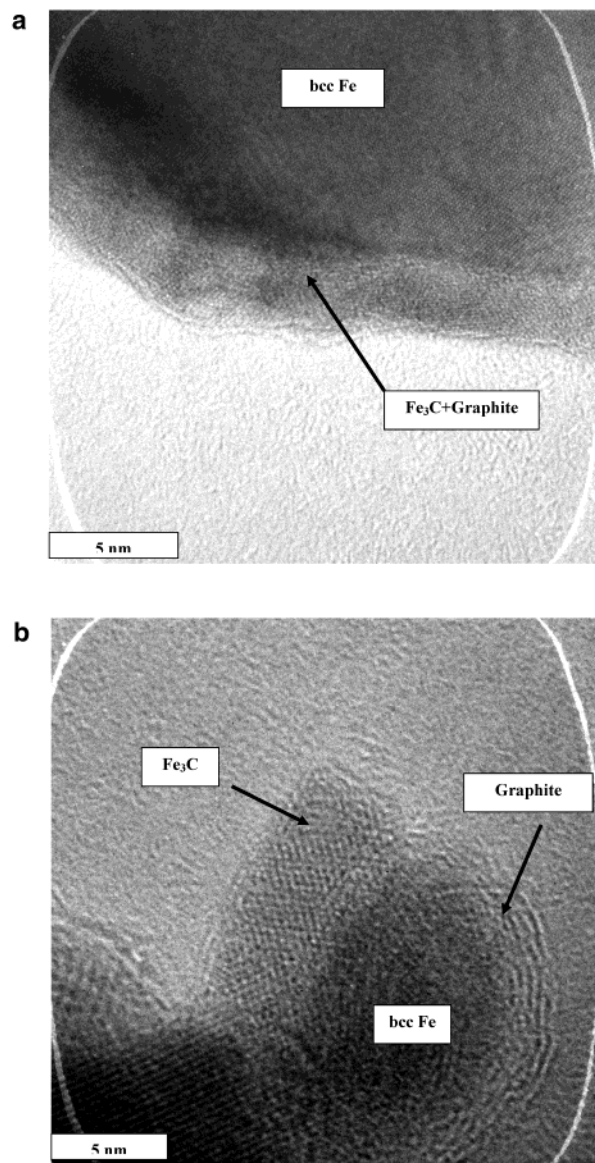

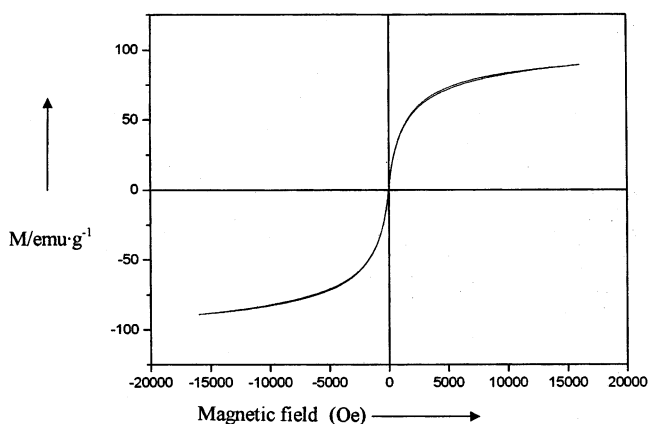**Figure 8.** High-resolution TEM image of the particles annealed at 700 °C.

Figure 9. Magnetization curve of as-prepared material.

concentration decreases. At the same time, the overheated material (850 °C during 5 h) without a significant content of Fe₃C exhibits a relatively low M_s value.

The decrease in coercivity with the temperature of annealing agrees with the change of the magnetic ground state of Fe nanoparticles from single-domain to multidomain due to the

7626 *J. Phys. Chem. B, Vol. 108, No. 23, 2004*

Nikitenko et al.

TABLE 5: Magnetic Properties[c] of Iron Nanoparticles, Measured at Room Temperature

temp of annealing	M_S (10^6 A m^{-1})	M_R (10^5 A m^{-1})	H_C (Oe)
300	0.74	2.5	450
400	1.2	0.52	180
700	1.62	0.29	40
800	1.82	0.11	4.0
850[a]	1.36	0.46	50
700[b]	0.54	7.9	250

[a] Annealing time was 5 h. [b] As-prepared sample was synthesized by sonication at 90 °C. [c] Please note that the estimated error in M_S and M_R is at least 10%.

increase in their size (see Tables 4 and 5). This change in turn alters the mechanism of coercivity from the rotation of magnetization in single-domain particles to domain wall motion in multidomain particles that may result in the noted dropping of H_C.[25] The decrease of the coercivity with annealing temperature also can be related to the reduction of Fe_3C concentration, since the H_C value of Fe_3C is higher than that of bcc-Fe.[26]

The chemical composition of prepared Fe/Fe_3C nanocrystalline particles with the best magnetic properties is close to that of ordinary cast iron.[26,27] Magnetization of the cast iron is relatively low, since the M_S of the bulk Fe_3C (6.3×10^4 A m^{-1})[22] is much smaller than that of the bulk bcc-Fe (1.7×10^6 A m^{-1}). Despite this, the saturation magnetization of Fe/Fe_3C nanocrystalline particles obtained with sonochemistry is similar than that of bulk bcc-Fe. The magnetization of the sample enriched in Fe_3C, found to be equal to $5.4 \times 10^5 \pm 0.6 \times 10^5$ A m^{-1}, is also much higher than that expected from its composition ($\sim$30 mol % of Fe_3C). Thus, one can conclude that the enhanced magnetization of the obtained nanocrystalline material can be related to the magnetic interaction between the bcc-Fe in the core and the Fe_3C in the particle's shell. It is worth noting that iron nanocrystalline particles coated only with carbon or graphite[3,7] exhibit much lower magnetization.

Particles' Stability. As-prepared material is pyrophoric and must be handled in an inert atmosphere. Annealed materials do not show a visible change when exposed to air. The time stability of obtained nanocrystalline particles was tested by sequential measurements of Mössbauer spectra and the magnetization value. It was found that the samples annealed at 700−800 °C exhibit a strong resistance to oxidation. The MS spectra and M$_S$ values do not change after at least four months of contact with air. These results are in good agreement with the above-mentioned dc resistivity measurements. Particles are also stable at least for one week when in contact with water and a NaOH solution in ethanol. Treatment with 0.5 M HCl causes a rapid dissolution of annealed materials. It can be assumed that particle stability is caused by the protective shell from Fe_3C and partially from graphite.

Conclusions

(1) Sonolysis of $Fe(CO)_5$ in diphenylmethane in argon results in a pyrophoric amorphous solid product, which can be characterized as iron nanoparticles embedded in a polymeric matrix.

(2) Annealing of the as-prepared material in argon at temperatures up to 800 °C leads to the growth of air-stable iron nanocrystalline particles, coated by an iron carbide protective layer.

(3) Particle composition and their magnetic properties are controlled by annealing temperature and the conditions of sonochemical treatment.

(4) The saturation magnetization of annealed materials is close, or even higher, than that of bulk iron. This unusual phenomenon could be attributed to the specific magnetic interaction between bcc-Fe in the core and Fe_3C in the shell of the particles.

Supporting Information Available: Figures showing magnetization loops as a function of annealing temperature (PDF). This material is available free of charge via the Internet at http://pubs.acs.org.

References and Notes

(1) Litvinov, D.; Kryder, M. H.; Khizroev, S. *J. Magn. Magn. Mater.* **2001**, *232*, 84.

(2) Ripka, P. G. *J. Magn. Magn. Mater.* **2000**, *215−216*, 795.

(3) McHenry, M. E.; Majetich, S. A.; Artman, J. O.; De Graef, M.; Staley, S. W. *Phys. Rev. B* **1994**, *49*, 11358.

(4) McHenry, M. E.; Laughlin, D. E. *Acta Mater.* **2000**, *48*, 223.

(5) Carpenter, E. E. *J. Magn. Magn. Mater.* **2001**, *225*, 17.

(6) Hofmeister, H.; Huisken, F.; Kohn, B.; Alexandrescu, R.; Cojocaru, S.; Crunteann, A.; Morjan, I.; Diamandescu, L. *Appl. Phys. A* **2001**, *72*, 7.

(7) Murata, K.; Ushijima, H.; Uchida, K. *J. Jpn. Petr. Inst.* **1998**, *41*, 168.

(8) Babonneau, D.; Naudon, A.; Cabioch, T.; Lyon, O. *J. Appl. Crystallogr.* **2000**, *33*, 437.

(9) Tomita, S.; Hikita, M.; Fujii, M.; Hayashi, S.; Yamamoto, K. *Chem. Phys. Lett.* **2000**, *316*, 361.

(10) Wonterghem, J.; Morup, S.; Charles, S. W.; Wells, S.; Villadsen, J. *Phys. Rev. Lett.* **1985**, *55*, 410.

(11) Suslick, K. S.; Fang, M.; Hyeon, T. *J. Am. Chem. Soc.* **1996**, *118*, 11960.

(12) Nikitenko, S. I.; Koltypin, Yu.; Palchik, O.; Felner, I.; Xu, X. N.; Gedanken, A. *Angew. Chem., Int. Ed.* **2001**, *40*, 4447.

(13) Nikitenko, S. I.; Koltypin, Yu.; Markovich, V.; Rosenberg, E.; Gorodetsky, G.; Gedanken, A. *IEEE Trans. Magn.* **2002**, *38*, 2592.

(14) Mason, T. J. *Chemistry with Ultrasound*; Elsevier: New York, 1990.

(15) Nikitenko, S. I.; Koltypin, Yu.; Pickup, D.; Van Eck, E.; Gedanken, A. *Ultrason. Sonochem.* **2003**, *10*, 11.

(16) Nakanishi, K.; Solomon, H. *Infrared Absorption Spectroscopy*; Holden-Day, Inc., San Francisco, 1982.

(17) Suslick, K. S.; Choe, S. B.; Cicholas, A. A.; Grinstaff, M. W. *Nature* **1991**, *353*, 414.

(18) Cao, X.; Koltypin, Yu.; Kataby, G.; Prozorov, R.; Gedanken, A. *J. Mater. Res.* **1995**, *10*, 2952.

(19) Gross, R.; Alff, L.; Büchner, B.; Freitag, B. H.; Höfener, C.; Klein, J.; Yafeng, Lu,; Mader, W.; Philipp, J. B. R.; Rao, M. S.; Reutler, P.; Ritter, S.; Thienhaus, S.; Uhlenbruck, S.; Wiedenhorst, B. *J. Magn. Magn. Mater.* **2000**, *211*, 150.

(20) Balcells, L. I.; Fontcuberta, J.; Martinez, B.; Obradors, X.; *Phys. Rev. B* **1998**, *58*, R14697.

(21) Dong, X. L.; Zhang, Z. D.; Xiao, Q. F.; Zhao, X. G.; Chuang, Y. C.; Jin, S. R.; Sun, W. M.; Li, Z. J.; Zheng, Z. X.; Yang, H. *J. Mater. Sci.* **1998**, *33*, 1915.

(22) Jiao, J.; Seraphi, S.; Wang, X.; Withers, J. *J. Appl. Phys.* **1996**, *80*, 103.

(23) Robertson, J. *Adv. Phys.* **1986**, *35*, 317.

(24) Meyerson, B.; Smith, F. W. *J. Non-Cryst. Sol.* **1980**, *35*, 435.

(25) Kodama, R. H. *J. Magn. Magn. Mater.* **1999**, *200*, 359.

(26) *Metals Handbook*, 9th ed., *9*: *Metallography and Microstructures*; Metal Park, OH, 1985.

(27) Cullity, B. D. *Introduction to Magnetic Materials*; Addison-Wesley Publishing: Reading, MA, 1972.